

# Chapter 12

## Generalized Continua Concepts in Coarse-Graining Atomistic Simulations



Shuozhi Xu, Ji Rigelesaiyin, Liming Xiong, Youping Chen  
and David L. McDowell

**Abstract** Generalized continuum mechanics (GCM) has attracted increased attention in the context of multiscale materials modeling, an example of which is a bottom-up GCM model, called the atomistic field theory (AFT). Unlike most other GCM models, AFT views a crystalline material as a continuous collection of lattice points; embedded within each point is a unit cell with a group of discrete atoms. As such, AFT concurrently bridges the discrete and continuous descriptions of materials, two fundamentally different viewpoints. In this chapter, we first review the basics of AFT and illustrate how it is realized through coarse-graining atomistic simulations via a concurrent atomistic-continuum (CAC) method. Important aspects of CAC, including its advantages relative to other multiscale methods, code development, and numerical implementations, are discussed. Then, we present recent applications of CAC to a number of metal plasticity problems, including static dislocation properties, fast moving dislocations and phonons, as well as dislocation/grain boundary interactions. We show that, adequately replicating essential aspects of dislocation fields at a fraction of the computational cost of full

---

S. Xu

California NanoSystems Institute, University of California, Santa Barbara,  
Santa Barbara, CA 93106-6105, USA

J. Rigelesaiyin · L. Xiong

Department of Aerospace Engineering, Iowa State University, Ames, IA 50011, USA

Y. Chen

Department of Mechanical and Aerospace Engineering, University of Florida,  
Gainesville, FL 32611-6250, USA

D. L. McDowell

Woodruff School of Mechanical Engineering, Georgia Institute of Technology,  
Atlanta, GA 30332-0405, USA

D. L. McDowell (✉)

School of Materials Science and Engineering, Georgia Institute of Technology,  
Atlanta, GA 30332-0245, USA

e-mail: david.mcdowell@me.gatech.edu

atomistics, CAC is established as an effective tool for coarse-grained modeling of various nano/micro-scale thermal and mechanical problems in a wide range of monatomic and polyatomic crystalline materials.

## 12.1 Generalized Continuum Mechanics (GCM)

In classical continuum mechanics (CCM), a material consists of continuously distributed material points with infinitesimal size that fill the entire region of an infinite space they occupy [1]. The micro-scale kinetics or dynamics are implicitly averaged. The physical properties of each point are determined only by the deformation and history of that point, i.e., each point behaves independently following the same constitutive law. Interactions between these points take place only through the balance equations. Mechanics of real materials, however, deals with finite-sized materials with finite-sized material points, e.g., a large number of molecules, or the primitive unit cell of a crystal. From the atomic viewpoint, there is a lower limit to divisibility for any material, as continuum quantities such as mass density only have physical meaning in regions actually containing matter. Thus, CCM fails to describe the materials deformation at the atomic/nano-scale.

Limitations of CCM have motivated the development of various enhanced methods, a vast number of which aim at tackling the locality issue. Among these methods, a weakly nonlocal theory, named generalized continuum mechanics (GCM, also known as microcontinuum field theory), extends the classical field theory to microscopic space and time scales [2]. In GCM, materials are envisioned as a continuum collection of deformable point particles. Each point particle, with a finite size, has a continuous internal deformation which is represented by some vectors attached to it. Accordingly, a particle is identified by its position vector  $\mathbf{R}$  and some director vectors attached to this point  $\mathbf{\Xi}_\alpha$  in the undeformed state. In a solid crystal,  $\mathbf{R}$  is employed to describe the continuous lattice deformation, in which the material is viewed as a collection of infinitesimal point particles, while  $\mathbf{\Xi}_\alpha$  considers each point particle with finite size and describes its continuous internal deformation. Both  $\mathbf{R}$  and  $\mathbf{\Xi}_\alpha$  have their own motions or mappings to the deformed states  $\mathbf{r}$  and  $\xi_\alpha$  at time  $t$ , respectively, i.e.,

$$\mathbf{R} \rightarrow {}^t\mathbf{r}, \mathbf{\Xi}_\alpha \rightarrow {}^R, {}^t\xi_\alpha, \alpha = 1, 2, 3, \dots, N \quad (12.1)$$

Such a medium is called microcontinuum of grade  $N$ . By introducing  $\mathbf{\Xi}_\alpha$ , the microcontinuum naturally brings length and time scales into the field theories; by considering the ratio of the external characteristic length to the internal characteristic length, the GCM theories are nonlocal in character. For the first grade microcontinuum ( $N = 1$ ),  $\mathbf{\Xi}_1$  are three deformable directors, conferring each point particle nine extra degrees of freedom (DOFs) compared to the local theory. This is the micromorphic continuum. The other two are the microstretch continuum and the

micropolar continuum, which can be achieved by constraining the director vectors in certain ways.

In the last seven years, Maugin [1–7] dedicated an extensive effort to the understanding and dissemination of GCM by offering a historical perspective, deep mathematical and physical insights, as well as a clear explanation of its essences. Maugin [3] summarized and discussed three possible paths towards the generalization of continuum mechanics: “*involving an additional microstructure at each material point*”, “*introducing higher order gradients of the displacement in the energy density (weak nonlocal theory)*”, and “*considering spatial functionals for the constitutive equations (strongly or truly nonlocal theory)*”. Maugin [3] further posited and addressed three questions: “(1) *Do we need GCM at all?* (2) *Do we find the necessary tools in what exists nowadays?* (3) *What is the relationship between discrete and continuous descriptions if there must exist a consistent relationship between the two?*”

For the third question, Maugin [3] wrote “*the author personally believes that any relationship that can be established with a sub-level degree of physical description is an asset that no true physicist can discard*”. This perspective is based on the distinction between atomic and continuous descriptions of matter; for the former, matter is manifested as discrete particles, whereas for the latter, matter is infinitely divisible. These two different views lead to fundamentally different theories. The “*material point*”, Maugin [2] wrote, “*is quite suspiciously defined in a classical continuum*”; “*A point is the intersection of two immaterial (zero-thickness) curves on a two-dimensional surface. This, Newton already knew in his ‘Principia Mathematica’ where mass at a so-called ‘material point’ can only be defined by density multiplied by volume*”. To avoid introducing the physical concept of a material point, CCM textbooks use global conservation laws to derive the local balance laws by purely mathematical means, leaving the question on the conditions under which the differential form of balance laws are valid unanswered. While continuum physics is always an approximation to the underlying discrete molecular physics, GCM is undoubtedly a better approximation than CCM to the description of real materials. It helps to bridge the gap between continuum and atomic views of materials.

## 12.2 Atomistic Field Theory (AFT)

In micromorphic field theory, the motion of point particles is governed by conservation equations of mass, microinertia, generalized spin, linear momentum, and energy. Based on micromorphic field theory, Chen and Lee [8] proposed a new GCM model, called the atomistic field theory (AFT), which treats a crystalline material as a continuous collection of material points (unit cells), but with each material point possessing internal DOFs that describe the movement of atoms inside each unit cell, as shown in Fig. 12.1. In this way, the micromorphic theory is

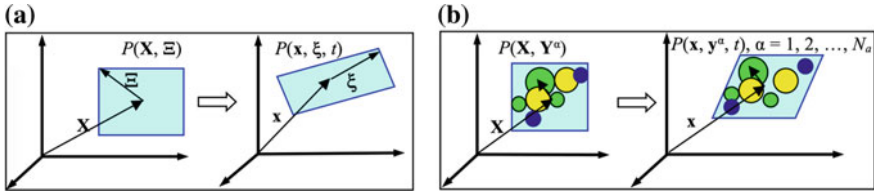


**Fig. 12.1** Macro- and micro-motions of a material particle  $P$  in **a** micromorphic theory and **b** AFT. Left in **a** and **b** is the reference state at time 0 while right is the deformation state at time  $t$ .  $\mathbf{X}$  and  $\mathbf{x}$  are the positions of the mass center of the unit cell,  $\Xi$  and  $\xi$  are internal positions,  $\mathbf{Y}^\alpha$  and  $\mathbf{y}^\alpha$  are positions of atom  $\alpha$  with respect to  $\mathbf{X}$  and  $\mathbf{x}$ , respectively,  $N_a$  is the number of atoms in a unit cell. Reproduced with permission from Ref. [11]

connected with molecular dynamics (MD) and encompasses the atomic scale [9]. Here, the local density function is continuous at the level of the unit cell, but discrete in terms of the discrete atoms inside the unit cell [10, 11].

AFT differs from CCM in that it has two-level structure description of materials. It is also distinct from popular generalized continuum theories, such as the Cosserat theory [12], micropolar theory, [13, 14], micromorphic theory [15–20], or other generalized continuum theories [21, 22], in that the sub-level structure and physical description are not continuous but discrete. As a result of the discrete sub-level description in AFT, only balance of linear momentum is relevant to the dynamics. A comparison of the material description in AFT with those in GCM and CCM is presented in Table 12.1.

The main theoretical tool to link the atomic to the continuum description is statistical mechanics [23–26]. Statistical mechanics views thermodynamics and

**Table 12.1** Comparison of CCM, top-down formulated theories of GCM, and AFT

Theory	Material description	Constituents of materials	Internal DOF	Governing laws	Constitutive relations
CCM	A single phase single component continuum	0D Material point without structure	None	Conservation of mass, linear and angular momentum, and energy	11 constitutive relations
GCM	A continuum with embedded microstructure	Finite-sized material particles	3 in micropolar, 9 in micromorphic	Conservation of mass, micro-inertia, linear and angular momentum, generalized spin, and energy	20 constitutive relations
AFT	A crystal structure as lattice + basis	Atoms	$3 N_a$ ( $N_a$ is the number of atoms in one basis)	Conservation of mass, linear momentum, and energy	Interatomic potential

continuum mechanics as coarse-grained (CG) descriptions of classical  $N$ -body dynamics, and defines “coarse-graining” as “*the process of representing a system with fewer degrees of freedom than those actually present in the system*” [27]. From this definition, existing CG models are either atomistic CG models that are derived bottom-up from the underlying atomistic model or phenomenological models that have no direct connection to the underlying atomistic model. Existing coarse-graining methods for derivation of atomistic CG models can be further divided into three categories [11]: (1) reducing the order of particle representation of the molecular structure, e.g., the super-atom method, united-atom method, and multiscale-CG [28–31], (2) assuming continuous deformation of the lattice (affine or using some other imposed shape functions), e.g., quasicontinuum (QC) [32], hot-QC [33–35] and coarse-grained molecular dynamics (CGMD) [36], and (3) deriving an equivalent continuum field representation for the atomistic system, e.g., the Irving-Kirkwood (IK) statistical mechanics formulation of hydrodynamics [37], MD formulation of micromorphic theory [17–20], and the AFT formulation [8, 9]. These are shown in Table 12.2.

Different from other GCM theories that are derived via a top-down approach, AFT is bottom-up derived from the underlying atomistic model, and hence it is also a CG atomistic model. The AFT formulation is an extension of the IK formulation of “*the hydrodynamics equations for a single component, single phase system*” [37] to a two-level structural description of general crystalline materials. It employs the two-level crystalline materials description in solid state physics, i.e., crystal structure = lattice + basis [38]. As a result of its bottom-up atomistic formulation, all the

**Table 12.2** Comparison of atomistic CG methods. ODE and PDE stand for ordinary differential equations and partial differential equations, respectively

Atomistic CG methods	Route to CG	Entities in simulations	Representative CG models	Governing laws	Governing equations
Structural reduction	From atoms to super-atoms through grouping many atoms into one super-atom	Super-atoms	Super-atom method, united atom method, multiscale-CG [28–31]	Newtonian Mechanics	2nd order ODE
Assuming homogeneous displacements of atoms	From atoms to rep-atoms using the Cauchy-Born rule or other prescribed shape functions	Representative atoms	QC [32], hot-QC [33–35]	Energy minimization	1st order ODE
Using continuum representation	From atomistic to continuum using statistical mechanics	Material points	IK hydrodynamics [37], AFT [8, 9]	Conservation laws	2nd order PDE

essential atomistic information of the material, including the atomic-level crystal structure and the interactions between atoms, is attained. The formulation naturally leads to a concurrent atomistic-continuum representation of the materials governed by a single set of balance equations for both atomic and continuum regions, as an exact consequence of Newton's second law [8, 9], in the following forms,

$$\frac{d\rho^\alpha}{dt} + \rho^\alpha (\nabla_{\mathbf{x}} \cdot \mathbf{v} + \nabla_{\mathbf{y}^\alpha} \cdot \Delta \mathbf{v}^\alpha) = 0 \quad (12.2)$$

$$\rho^\alpha \frac{d}{dt} (\mathbf{v} + \Delta \mathbf{v}^\alpha) = \nabla_{\mathbf{x}} \cdot \mathbf{t}^\alpha + \nabla_{\mathbf{y}^\alpha} \cdot \boldsymbol{\tau}^\alpha + \mathbf{f}_{\text{ext}}^\alpha \quad (12.3)$$

$$\rho^\alpha \frac{de^\alpha}{dt} = \nabla_{\mathbf{x}} \cdot \mathbf{q}^\alpha + \nabla_{\mathbf{y}^\alpha} \cdot \mathbf{j}^\alpha + \mathbf{t}^\alpha : \nabla_{\mathbf{x}} (\mathbf{v} + \Delta \mathbf{v}^\alpha) + \boldsymbol{\tau}^\alpha : \nabla_{\mathbf{y}^\alpha} (\mathbf{v} + \Delta \mathbf{v}^\alpha) \quad (12.4)$$

where  $\mathbf{x}$  is the physical space coordinate of the continuously distributed lattice;  $\mathbf{y}^\alpha$  ( $\alpha = 1, 2, \dots, N_a$ ), with  $N_a$  being the total number of atoms in a unit cell, is the subscale internal variable describing the position of atom  $\alpha$  relative to the mass center of the lattice located at  $\mathbf{x}$ ;  $\rho^\alpha$ ,  $\rho^\alpha (\mathbf{v} + \Delta \mathbf{v}^\alpha)$ , and  $\rho^\alpha e^\alpha$  are the local densities of mass, linear momentum, and internal energy, respectively;  $\mathbf{v} + \Delta \mathbf{v}^\alpha$  is the atomic-level velocity and  $\mathbf{v}$  is the velocity field;  $\mathbf{f}_{\text{ext}}^\alpha$  is the external force field;  $\mathbf{t}^\alpha$  and  $\mathbf{q}^\alpha$  are the momentum flux and heat flux due to the homogeneous deformation of lattice, respectively;  $\boldsymbol{\tau}^\alpha$  and  $\mathbf{j}^\alpha$  are the momentum flux and heat flux due to the reorganizations of atoms within the lattice cells, respectively.

For conservative systems, i.e., in the absence of an internal source that generates or dissipates energy, the energy equation (Eq. 12.4) is equivalent to the linear momentum equation (Eq. 12.3). We remark that, supplemented with the interatomic force field, the first two AFT balance equations (Eqs. 12.2 and 12.3) are sufficient for a wide range of thermal and mechanical problems, some of which will be discussed in Sect. 12.4. Employing the classical definition of kinetic temperature, which is proportional to the kinetic part of the atomic stress, the linear momentum equations can be expressed in a form that involves the internal force density and temperature  $T$  [39–41], i.e.,

$$\rho^\alpha \ddot{\mathbf{u}}^\alpha(\mathbf{x}) + \frac{\gamma^\alpha k_B}{\Delta V} \nabla_{\mathbf{x}} T = \mathbf{f}_{\text{int}}^\alpha(\mathbf{x}) + \mathbf{f}_{\text{ext}}^\alpha(\mathbf{x}), \quad \alpha = 1, 2, \dots, N_a \quad (12.5)$$

where  $\mathbf{u}^\alpha(\mathbf{x})$  is the displacement of atom  $\alpha$  at point  $\mathbf{x}$ ; the superposed dots denote the material time derivative;  $\Delta V$  is the volume of the finite-sized material particle (the primitive unit cell for crystalline materials) at  $\mathbf{x}$ ;  $k_B$  is the Boltzmann constant;  $\gamma^\alpha = \rho^\alpha / \sum_{\alpha=1}^{N_a} \rho^\alpha$ , and  $\mathbf{f}_{\text{int}}^\alpha$  is the internal force density and is a nonlinear nonlocal function of relative atomic displacements. For systems with a constant temperature field or a constant temperature gradient, the temperature term in Eq. 12.5 can be considered as a surface traction on the boundary or a body force in the interior of the material,  $\mathbf{f}_T^\alpha(\mathbf{x})$  [40]. Denoting the finite element shape function as  $\Phi_\xi(\mathbf{x})$ , the Galerkin weak form of Eq. 12.5 can be written as

$$\int_{\Omega(\mathbf{x})} \Phi_{\xi}(\mathbf{x}) (\rho^{\alpha} \ddot{\mathbf{u}}^{\alpha}(\mathbf{x}) + \mathbf{f}_{\text{T}}^{\alpha}(\mathbf{x}) - \mathbf{f}_{\text{int}}^{\alpha}(\mathbf{x}) - \mathbf{f}_{\text{ext}}^{\alpha}(\mathbf{x})) d\mathbf{x} = 0 \quad (12.6)$$

where  $\Omega(\mathbf{x})$  is the simulation domain; the integral, using Gaussian quadrature, can be approximated by a weighted sum of the evaluations of the integrand at a set of integration points, leading to a set of discretized governing equations with the finite element nodal displacement as the unknowns to be solved.

In summary, AFT coarse-grains a discrete atomistic model by introducing an equivalent continuum description, i.e., by formulating a GCM representation of the underlying atomistic model. The field equations are then discretized and solved using finite element method (FEM). This process can be interpreted using Maugin's insightful and inspirational remarks: "*continualization*" is "*to construct sensible models*"; "*discretization*" is "*to be able to solve problems*" [2].

## 12.3 The Concurrent Atomistic-Continuum (CAC) Method

### 12.3.1 A Comparison Between CAC and Other Multiscale Methods

The AFT-based concurrent atomistic-continuum (CAC) method outlined in this chapter is an integral finite element approach for coarse-grained atomistics that admits description of dislocation nucleation, migration, and interaction with or without adaptive coarse-graining [9, 42–44], in contrast to QC. A CAC model, in general, has two domains: an atomistic domain containing atoms and a coarse-grained domain containing elements, as shown in Fig. 12.2. CAC employs a unified atomistic-continuum integral formulation (Eq. 12.6) with elements that have discontinuities between them and an underlying nonlocal interatomic force-displacement relation as the only constitutive relation. Ghost forces arising from a change of the underlying continuum formulation and energy summation rules in other approaches based on domain decomposition or coarse-graining are not an issue in CAC since the underlying integral formulation and constitutive framework do not change. Dislocations can be modeled throughout the entire domain, whether at full atomistic resolution or coarse-grained, because the elements are assumed to have faces on slip planes of the lattice, e.g.,  $\{111\}$  and  $\{110\}$  planes in face-centered cubic (FCC) and body-centered cubic (BCC) lattices, respectively. This sets it apart from methods that require full atomistic resolution at the dislocation core. In contrast to QC, which has the objective of seeking convergence of the adaptively coarse-grained solution to that of the full atomistic solution for various field problems, CAC can have multiple purposes. On the one hand, it can coarse-grain in regions away from atomistic domains of interest and capture

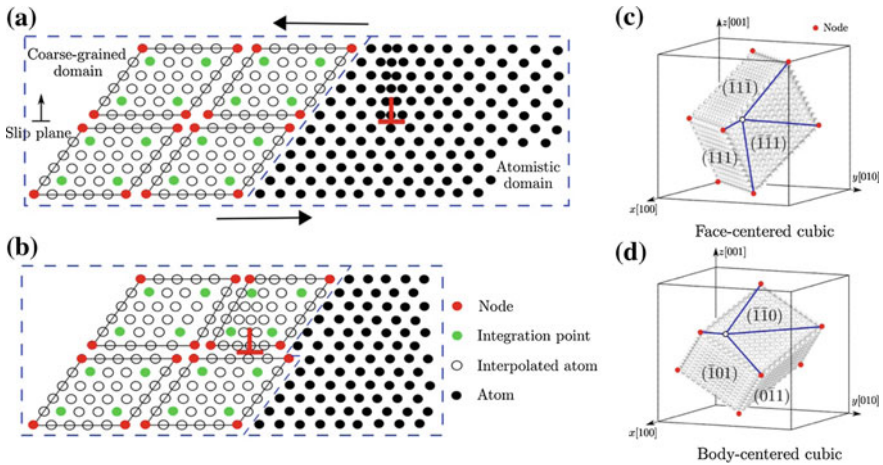


**Fig. 12.2 a–b** A 2-D CAC simulation domain consisting of an atomistic domain (right) and a coarse-grained domain (left). The atomistic domain is composed of atoms (black circles), which follow the same governing equations in the atomistic simulation. The coarse-grained domain consists of elements of varying size that have discontinuities between them, each of which contains a large number of underlying atoms with the nodes (red circles) as the only DOFs. Only the force/energy on integration points (green circles) and nodes are calculated. In **a**, an edge dislocation (red  $\perp$ ) is located in the atomistic domain. Upon applying a shear stress on the simulation cell, the dislocation migrates into the coarse-grained domain in **b**, where the Burgers vector spreads out between elements. **c–d** In 3-D, elements have faces on  $\{111\}$  planes and on  $\{110\}$  planes in an FCC and a BCC lattice, respectively. The positions of atoms within each element (open circles) are interpolated from the nodal positions. Reproduced with permission from Ref. [43]

long-range fields of dislocations, as in coupled atomistic and discrete dislocation (CADD) [45, 46]. On the other hand, it can model dislocations across a range of length scales to access trends and provide support for mechanistic understanding of coarse scale behavior of fields of dislocations, smearing individual cores but preserving the net Burgers vector, representing long-range and approximating short-range interactions. While QC typically seeks the most accurate and efficient solution to dislocation plasticity via adaptive remeshing of the domain near dislocations to full atomistic resolution, CAC can resolve full atomistics if necessary near interfaces or crack tips, but allows dislocations to nucleate, multiply, migrate, and interact even in the coarse-grained domain along interfaces between elements, introducing the option to coarse-grain dislocation fields over larger scales.

Like QC, CAC employs the same interatomic potential in both coarse-grained and atomistic domains where dislocations evolve and interact. This introduces systematic coarse-graining error, which originates from displacement approximation (i.e., the shape function) and the numerical integration. As the element size is reduced, the CAC predictions properly converge to the fully atomistic results. The coarse-graining error can be quantified and balanced with the high computational demands of remeshing, according to the purposes of the mesoscale modeling, for example in representation of dislocation core structures and short-range

interactions. It can also be minimized by use of adaptive remeshing, based on the level of the nodal displacement between elements [47]; this is necessary for general field problems to allow dislocation migration along arbitrary extended slip planes. However, remeshing need not be carried out to fully atomistic level, but can involve simply splitting larger continuum elements containing many atoms. Unlike QC, CAC does not employ the assumption of continuous lattice deformation throughout the coarse-grained domain and admits dislocation activity/displacement discontinuity between elements. As such, it pursues gradual coarse-graining from full atomistic resolution upward. For example, if trends of behavior or collective mechanisms are to be considered as a function of microstructure or stress state, as is often the case in applications of dislocation dynamics (DD) models [48–57], CAC may offer a means to support such parametric studies.

### 12.3.2 Code Development

The first version of the CAC numerical tool was developed by Xiong and Chen [57, 58] and Deng et al. [39, 59]. The reformulated balance equations [9] were numerically implemented using FEM with trilinear finite element shape functions and nodal integration. Later, the form and capabilities of the CAC method were extended substantially in modeling quasistatic and dynamics behavior of dislocations: elements that have discontinuities between them were employed, and the Gaussian quadrature was used for integration in the coarse-grained domain [42, 60–66]. Yang et al. [67–70] rewrote the CAC code for multiscale simulation of polycrystalline ionic materials. Based on this code, Chen et al. [71–74] extended the CAC method for space- and time-resolved simulation of the transient processes of the propagation of heat pulses in single crystals and across GBs [72] as well as the interactions between heat pulses and moving dislocations [71]; a new shape function was designed to facilitate the seamless passing of waves between the atomistic and coarse-grained domains [73]. More recently, Xu et al. [44] developed PyCAC, a novel numerical implementation of the CAC approach. In PyCAC, the CAC method is implemented in Fortran 2008 with a distributed-memory spatial decomposition parallel algorithm, while a Python scripting interface is built to provide a robust user interface to facilitate parametric studies via CAC simulations without interacting with the underlying Fortran code and to improve handling of input, output, and visualization options. For example, the finite element nodal positions obtained in CAC simulations can be mapped back to atomic positions through the Python interface; in this way, the atomic trajectories can be visualized using common atomistic configuration viewers such as AtomEye [75] and OVITO [76]. It has been demonstrated that the PyCAC code has a good parallel scaling performance and is an efficient, user-friendly, and extensible CAC simulation environment [44].

### 12.3.3 Numerical Implementations in PyCAC

The PyCAC code [44] can simulate monatomic pure FCC and pure BCC metals using the Lennard-Jones [77] and the many-body embedded-atom method (EAM) [78] interatomic potentials in a constant temperature field. The energy equation (Eq. 12.5) and the term  $\mathbf{f}_T^\alpha$  (Eq. 12.6) have not yet been implemented because they have small effects on mechanical response in the case of constant temperature. We remark that (i) there is ongoing work in interpreting  $\mathbf{f}_T^\alpha$  and in comparing different descriptions of temperature in the coarse-grained domain [25, 26], and (ii) for monatomic crystals ( $N_\alpha = 1$ ),  $\mathbf{y}^\alpha$  vanishes, and atom  $\alpha$  sits at the nodal site; Eqs. 12.2–12.4 reduce to the balance equations in CCM.

In the coarse-grained domain, the integral in Eq. 12.6 is approximated using Gaussian quadrature, in which the positions and weights of the integration points are usually determined by the order of the integrand. It is, however, difficult to employ a unified set of integration points within an element because that the interatomic potential-based  $\mathbf{f}_{\text{int}}^\alpha(\mathbf{x})$  can be a complicated and highly non-linear function and that the variation of the integrand is not uniform within an element [43, 79]. To circumvent this problem, each element is divided into a number of non-overlapping subregions. In this way, one only needs to determine the order of the integrand within each subregion, which is usually lower than that within the entire element and is more easily approximated. In practice, either the first order [42] or the second order [43] Gaussian quadrature can be adopted, with a trilinear shape function  $\Phi_\xi(\mathbf{x})$ , and the force on node  $\xi$  is

$$\mathcal{F}^\xi = \frac{\sum_\mu \omega_\mu \Phi_{\mu\xi} \mathbf{F}^\mu}{\sum_\mu \omega_\mu \Phi_{\mu\xi}} + \mathbf{F}_{\text{ext}}^\xi \quad (12.7)$$

where  $\omega_\mu$  is the weight of integration point  $\mu$ ,  $\Phi_{\mu\xi}$  is the shape function of node  $\xi$  at integration point  $\mu$ ,  $\mathbf{F}^\mu$  is the interatomic potential-based atomic force on integration point  $\mu$ , and  $\mathbf{F}_{\text{ext}}^\xi$  is the external force applied on node  $\xi$ . We refer the readers to Refs. [43, 79] where details of the Gaussian quadrature, subregion, and integration points are presented.

In the atomistic domain, an atom can be viewed as a special finite element for which the shape function  $\Phi_\xi$  in Eq. 12.6 reduces to 1 at the atomic site, and the force on atom  $\alpha$  is simply

$$\mathbf{F}^\alpha = -\nabla_\alpha E + \mathbf{F}_{\text{ext}}^\alpha \quad (12.8)$$

where  $E$  is the interatomic potential-based internal energy and  $\mathbf{F}_{\text{ext}}^\alpha$  is the external force applied on atom  $\alpha$ . As such, common atomistic simulation techniques are employed: Newton's third law is employed to promote efficiency in calculating the force, pair potential, local electron density, and stress; the short-range neighbor search employs a combined cell list [80] and Verlet list [81] method.

Distinguished by how  $\mathcal{F}$  and  $F$  are subsequently used, two main types of CAC simulations—dynamic CAC and quasistatic CAC, by analogy with MD and molecular statics (MS), respectively—have been developed. In dynamic CAC, the equation of motion (Eq. 12.6) or its modified form of each node/atom is solved directly using the velocity Verlet algorithm [82]. In quasistatic CAC,  $\mathcal{F}$  and  $F$  are used to adjust the nodal and atomic positions, respectively, at each increment of system loading during energy minimization. For example, in both conjugate gradient and steepest descent algorithms,  $\mathcal{F}$  and  $F$  are taken as the initial directions along which the nodes and atoms should move, respectively [43]. In practice, a third type of CAC simulation—hybrid CAC—can be employed to perform periodic energy minimization during a dynamic CAC simulation, so as to enable the constrained multiscale optimization for a sequence of non-equilibrium defect configurations in materials [83, 84]. In all types of CAC simulations, the nodes in the coarse-grained domain and the atoms in the atomistic domain interact with each other at each simulation step and are updated concurrently. More specific details of PyCAC, including the input script format and a few example problems, can be found in the PyCAC user’s manual that is hosted on [www.pycac.org](http://www.pycac.org).

## 12.4 Applications of the CAC Method to Metal Plasticity

Metal plasticity is a multiscale phenomenon that is manifested by irreversible microstructure rearrangement associated with nucleation, multiplication, interaction, and migration of dislocations [85]. Long-range field interactions between dislocations, along with the short-range dislocation reactions, are extremely important to describe in predicting the overall plastic behavior of materials at the macroscopic level. The former necessitates large solution scales, while the latter demands treatment of core effects using accurate underlying interatomic potentials. Metal plasticity therefore requires concurrent coupling across various scales.

In the context of dislocation/crack mediated metal plasticity, CAC has been used in a number of applications. These include impact of a rigid ball against a plate in an ideal FCC single crystal [59] and a SrTiO<sub>3</sub> polycrystal [69], brittle fracture in an ideal FCC crystal [39] and SrTiO<sub>3</sub> [67], ductile fracture in Cu [47], dislocation nucleation from notched specimens in Cu, Ni, and Al [42, 60, 61], nanoindentation in Cu [43, 60] and SrTiO<sub>3</sub> [67], nucleation and growth of dislocation loops in Cu, Al, and Si [62, 63], dislocation nucleation from GBs in SrTiO<sub>3</sub> [69], crack/GB interactions in SrTiO<sub>3</sub> [68], stationary dislocations in Cu, Ni, and Al [43, 86], quasistatic [43], subsonic [47], and transonic [66] dislocation migration in Cu, Ni, and Al, quasistatic dislocation migration across the atomistic/coarse-grained domain interface in Cu and Al [43], screw dislocation cross-slip in Ni [87], edge dislocations bowing out from obstacles in Al [88], dislocation multiplication from Frank-Read (FR) sources in Cu, Ni, and Al [86], dislocation/void interactions in Ni [65], dislocation/stacking fault interactions in Ni, Al, and Ag [89], sequential transfer of curved dislocations across GBs in Cu, Al, and Ni [83, 84], dislocation/phonon interactions in Cu [66, 71] and

Ni [64], phonon waves passing the atomistic/coarse-grained domain interface in 1D monatomic, diatomic, and triatomic crystals [90] and Cu single crystals [73], as well as phonon heat transport across a  $\Sigma 19$  symmetric tilt grain boundary (STGB) in Cu polycrystals [72]. The success of these calculations suggests the viability of using CAC simulations to study metal plasticity phenomena in a sufficiently large 3D model, which would normally be inaccessible to atomistics.

We remark that applications to date of the quasistatic CAC implementation [43] have been limited to monatomic crystals [43, 44, 79, 83, 84, 86, 87, 88, 89], while polyatomic crystals have been considered in dynamic CAC applications [57, 58, 62, 67, 68, 69, 70, 90]. Nevertheless, there is no theoretical challenge in applying quasistatic CAC to polyatomic crystals. The quasistatic implementation is considered useful for modeling reaction pathways for thermally activated dislocation processes in a manner that avoids the overdriven character of dynamic simulations. Hybrid CAC, with periodic energy minimization (e.g., every 50 time steps) while using quenched dynamics at each time step, may be regarded to accord with the concept of a sequence of constrained equilibrium states as espoused in internal state variable theory [91, 92], traversing the energy landscape such that each stage of the process (even with no dislocation flux) corresponds to a non-zero thermodynamic force (the Peach-Koehler force on a dislocation), due to elastic interactions. In the following, we discuss applications of the CAC method to static dislocation properties, fast moving dislocations and phonons, as well as dislocation/GB interactions.

### 12.4.1 *Static Dislocation Properties*

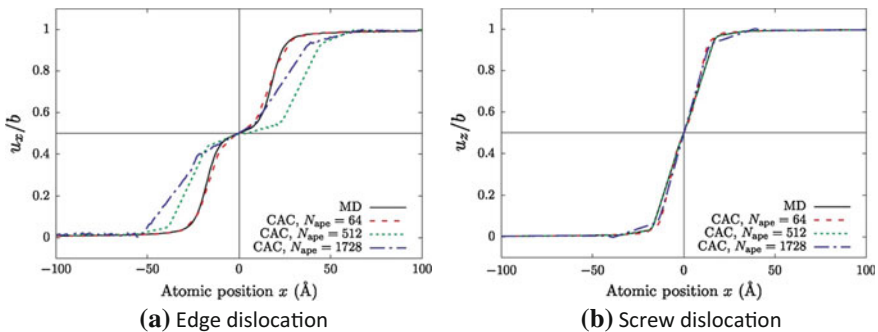
A question arises as to how well the non-singular dislocation core and associated Burgers vector [93–95] are described in the coarse-grained domain in CAC. For this purpose, quasistatic CAC simulations have been carried out to study certain benchmark problems, including generalized stacking fault energy (GSFE) [43], dislocation core structure/energy/stress fields [43, 86], and Peierls stress [86]. It is found that the coarse-grained domain predicts a less relaxed dislocation core. As a result, compared with atomistics, the coarse-grained domain exhibits a wider stacking fault width [43], a lower SFE [43], a larger core radius [86], a higher core energy [86], a lower Peierls stress [86], and a lower critical shear stress for dislocation bowing-out between obstacles [86, 88]; a dislocation also changes its local structure when passing across the numerical atomistic/coarse-grained domain interface [43].

To further understand the representation of dislocations in the coarse-grained domain in CAC, we calculate the disregistry and distribution of the Nye tensor [95, 96] around an edge and a screw dislocation in Cu. The fully coarse-grained simulation cell, with a size of  $180 \text{ nm} \times 32 \text{ nm} \times 6.5 \text{ nm}$  along the  $x$ ,  $y$ , and  $z$  direction, respectively, contains about 3 million atoms; periodic boundary conditions (PBCs) are applied along the dislocation line direction, i.e., the  $z$  direction, while the  $x$  and  $y$  boundaries are assumed traction free. The interatomic interactions are

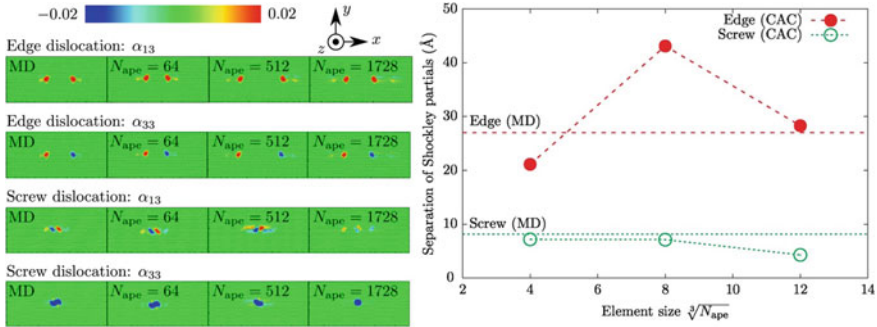
described using an EAM potential [97], which gives an equilibrium lattice constant  $a_0 = 3.615 \text{ \AA}$ . After displacing some nodes/atoms by  $b = (\sqrt{2}/2)a_0$  along a  $\langle 110 \rangle$  direction on a  $\{111\}$  plane, a damped dynamic CAC simulation [42] is conducted for 1 million steps with a time step of 1 fs at a near zero temperature to achieve an equilibrium full dislocation, which is dissociated into two Shockley partial dislocations with an intrinsic stacking fault in between [93, 94]. For comparison, damped MD simulations are also performed using LAMMPS [98]. Based on the interpolated atomic positions in the CAC simulations or the atomic positions in the MD simulations, the disregistry along the Burgers vector direction and the Nye tensor  $\alpha$  are calculated, the latter of which uses Atomsk [99] following Hartley and Mishin [100]. The calculations of  $\alpha$  are conducted on atoms within an area around the dislocation: 10 nm by 4.5 nm along the  $x$  and  $y$  axes, respectively; larger calculation areas do not change the results.

Figure 12.3 shows that there exists a linear correlation between disregistry and atomic position within an element, because of the trilinear shape/interpolation functions employed in the coarse-grained domain. For the Nye tensor  $\alpha$ , only  $\alpha_{13}$  and  $\alpha_{33}$  among the nine components are presented in Fig. 12.4 because they correspond to the edge and screw components of the partial dislocations, respectively. In both figures, with the smallest finite elements (64 atoms/element), results of the CAC simulations agree well with those of the MD simulations; with an increasing element size, the disregistry deviates and the separation between the two partial dislocations changes. Nevertheless, for the same dislocation, an integration of  $\alpha$  within the calculation area, i.e., the Burgers vector, yields identical result between CAC and MD, suggesting that the net Burgers vector (and so the long-range stress field) of a dislocation is indeed preserved in the coarse-grained domain in CAC.

We emphasize it is not our intent here to shed light on improved understanding of static dislocation core level phenomena, but rather to establish that CAC



**Fig. 12.3** Disregistry—the difference in the dislocation-induced displacement fields between two layers of atoms across the slip plane—of the **a** edge and **b** screw dislocations in Cu; The results in CAC with varying element size are compared with those of MD.  $u_x$  and  $u_z$  are the disregistry components along the Burgers vector direction, i.e., the  $x$  and  $z$  directions in cases of the edge and screw dislocation, respectively.  $b = (\sqrt{2}/2)a_0$  is the magnitude of the Burgers vector of a dislocation, where  $a_0$  is the lattice constant



**Fig. 12.4** Left: Nye tensor distribution around an edge or a screw dislocation in Cu, colored by the magnitude of two components  $\alpha_{13}$  and  $\alpha_{33}$ . CAC simulations with different element size ( $N_{ape}$  is the number of atoms per element) are employed, with the MD results also shown for comparison. Right: Separation of Shockley partial dislocations (based on  $\alpha_{13}$ ) with respect to the element size, in the cases of an edge and a screw dislocation. Both quantities converge to MD (horizontal lines) as each element has a smaller  $N_{ape}$ . The partial dislocation is assumed to sit at the mass center of the all surrounding atoms with the corresponding Nye tensor component that is larger than half the maximum value among all atoms. The partial dislocation position is unambiguously decided because most atoms have a value that is very close to either the maximum value or 0

adequately replicates essential aspects of dislocation fields, laying solid foundations for more complicated dislocation-mediated metal plasticity problems. The coarse-graining errors in the static dislocation properties are not essential in certain cases, e.g., dislocation/GB interactions (Sect. 12.4.3), because the dislocation has a correct core structure once it migrates into the atomistic domain in which the dislocation/defect interactions to be investigated take place.

### 12.4.2 Fast Moving Dislocations and Phonons

While much is known about static dislocations, the physics of dislocations moving near and above the sonic velocity in crystals remains relatively lightly explored [93, 94]. A dislocation moving in a lattice excites atomic vibrations and emits acoustic phonons [101]. The friction created by these interactions slows down the dislocation motion and reduces the mean distance between adjacent dislocations, leading to a stronger coupling between the long-range stress fields than that for static dislocations [66]. CAC is well-suited to explore fast moving dislocations and phonons because it concurrently captures the highly nonlinear time-dependent atomic-scale dislocation cores and the long-range elastic fields away from the cores.

For a fast moving dislocation in an otherwise perfect lattice, Xiong et al. [66] reported that (i) subject to the same resolved shear stress, the coarse-grained domain predicts a higher dislocation velocity, a larger phonon wavelength, and a larger

magnitude of the dislocation core stress field oscillation than the atomistic domain due to the linear shape/interpolation functions employed in the elements, and (ii) a fast moving dislocation has a velocity-dependent asymmetric stress field in which the leading partial dislocation possesses a higher stress level than the trailing partial dislocation as a result of the emitted phonon waves. In 1D monatomic, diatomic, and triatomic crystals, Xiong et al. [90] confirmed that the coarse-grained domain is able to reproduce complete phonon branches. In dynamic CAC simulations of dislocation/void interactions, Xiong et al. [65] discovered an inertia-induced transition from the Hirsch looping mechanism to the shearing mechanism, with the result that a relatively large void ( $\sim 5$  nm in diameter), which is a strong barrier for quasistatic dislocations, can behave as a weak barrier to dislocation motions under high strain-rate dynamic conditions. By performing fully coarse-grained atomistic simulations of dislocation/phonon interactions, Xiong et al. [64, 66] and Chen et al. [71] found that (i) the sub-THz phonon drag coefficient on dislocation migration increases with the increase of phonon wave packet magnitudes or sizes but is insensitive to the incident angles [64], and (ii) phonons reduce the dislocation energy, with some energy lagging behind the decelerated dislocation or dispersed around the arrested dislocation through emission of secondary phonon waves [66, 71]. In Cu polycrystals, Chen et al. [72] showed that the phonon/GB interactions alter the phonon focusing direction and locally reconstruct the GB, as shown in Fig. 12.5.

However, the fact that a dislocation may have different mobility, phonon wavelength, and dislocation core stress field in atomistic and coarse-grained domains raises the question of how the interface between the atomistic and coarse-grained domain affects the phonon transport in CAC [74]. The outstanding issue of a spurious wave reflection problem at the atomistic/continuum domain interface, encountered by many domain decomposition multiscale modeling methods [48], is mainly caused by the differences in material descriptions and

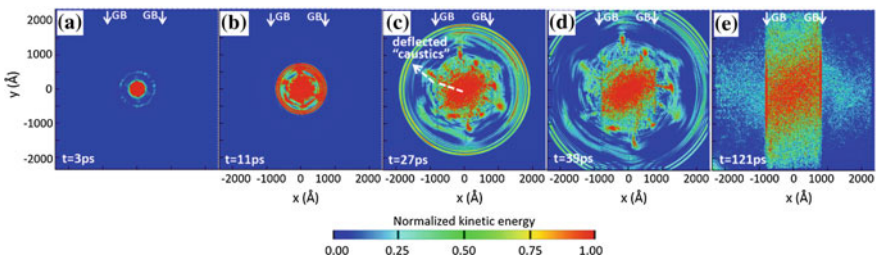


**Fig. 12.5** Time sequences of the normalized kinetic energy of transient heat flow in CAC simulations of a 2D Cu polycrystal. The GBs, rendered in full atomistic resolution, are indicated by white solid arrows. The phonons, with a wavelength of 5–250 nm, are generated in the simulation cell center using a coherent phonon pulse model [102]. With simultaneous ballistic and diffusive thermal transport, the phonon-focusing caustics are deflected by the GBs, which are indicated by the dashed white arrows in **c**. In **e**, only 60% of the total kinetic energy initially excited by the heat pulse is transmitted across the GBs; the phonon/GB interactions also give rise to the local GB structure change. Adapted with permission from Ref. [72]

governing equations between the atomistic and continuum models, which results in a mismatch in phonon dispersion relations. In CAC, due to the fact that coarse-graining cuts off short wavelength phonons [72, 73, 90], the phonon dispersion relations in the atomistic and coarse-grained domains overlap with each other only for wavevector that is smaller than a certain value. For this reason, CAC simulations of phonon/GB interactions [72] only involved medium- or long-wavelength phonons because the GB region is rendered in atomistic resolution. Recently, new shape/interpolation functions, different from the original trilinear ones, have been developed and applied to 1D elements to preserve the complete phonon information when a short-wavelength phonon seamlessly propagates across multiple atomistic/coarse-grained domain interfaces [73]. Work is underway to extend the new shape/interpolation functions to 2D and 3D for more complicated crystalline materials.

### 12.4.3 Dislocation/GB Interactions

The mechanism for slip transfer of lattice dislocations that migrate to and interact with GBs is one of the most pressing yet unresolved issues facing GB engineering and polycrystal plasticity [103]. Although in situ transmission electron microscope experiments capture the real-time dynamic process of slip transfer, they are unable to discern 3D atomic-scale events at the dislocation/GB interaction sites to yield quantitative information [104]. The multiscale nature of the sequential transfer of slip across GBs, in which both the atomic scale structure of the interface and the long-range fields of dislocation pile-ups are important, also poses challenges from the perspective of computational simulation [85]. For example, dislocation-based continuum approaches such as the crystal plasticity FEM (CPFEM) and rule-based DD are not readily applicable to simulate the interactions between dislocations and GBs because they usually do not naturally incorporate the necessary microscopic DOFs associated with the GBs and other evolving internal state variables that relate to detailed slip transfer criteria [48, 105]. On the other hand, atomistic simulations, which are preferred for understanding local GB structure-specific slip transfer responses, are limited by the size of the computational cell in considering the long-range stress field [106].

We performed hybrid CAC simulations [44] to study the sequential slip transfer of mixed character dislocations across a  $\Sigma 3\{111\}$  coherent twin boundary (CTB) in Cu, Ni, and Al [83, 84], as well as a  $\Sigma 11\{113\}$  STGB in Ni [84]. In all simulations, the GBs are rendered in full atomistic resolution while the coarse-grained domain is used to accommodate long distance migration of dislocation pile-ups, which are introduced either by multiplication from an FR source [83, 86] or Volterra knives [84], the latter case is shown in Fig. 12.6a. The dislocations then move towards the GB subjected to a constant applied shear stress.

For a  $\Sigma 3$  CTB in Cu and Al [83], it is found that, under a relatively small shear stress, (i) in Cu, the leading screw segment cuts into the twinned grain, i.e., the CTB

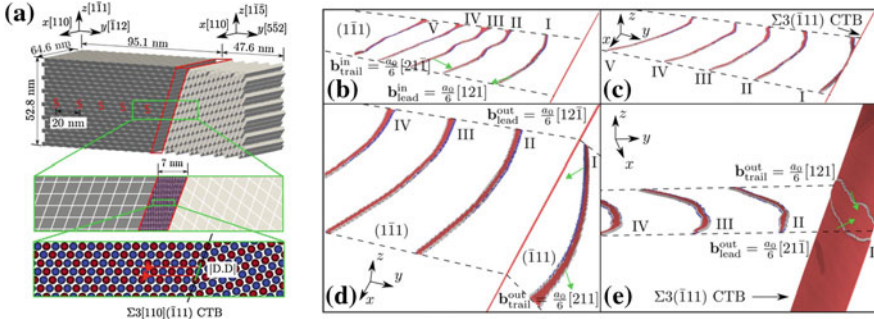


**Fig. 12.6** a Bicrystal simulation cells used to study sequential slip transfer of five  $(a_0/2)[110](111)$  dislocations (red S) across a  $\Sigma 3(111)$  CTB in Ni. An atomistic domain is meshed in the vicinity the CTB; the jagged interstices at the cell boundaries are also filled in with atoms, which are not shown here. Away from the GBs and cell boundaries are coarse-grained finite elements, each containing 2197 atoms. All cell boundaries are assumed traction free to allow a full 3D description. Exploded views of the GB region appear in the lower region, where atoms in different  $(110)$  atomic layers have different colors; the  $\Sigma 3$  CTB is composed of all D structural units, and so all sites along the CTB are equivalent for dislocation impingement. **b–e** Snapshots of dislocation pile-up with dominant leading screw character impinging against the CTB. Atoms are colored by adaptive common neighbor analysis [107]: red are of hexagonal-close packed local structure, blue are BCC atoms, and all FCC atoms are deleted. In **a** five incoming dislocations approach the CTB subject to an applied shear stress. In **b** the leading dislocation is constricted at the CTB, where two Shockley partial dislocations are recombined into a full dislocation. In **c** with Mishin-EAM [108] and Voter-EAM [109] potentials, the dislocation effectively cross-slips into the outgoing twinned grain via redissociation into two partials. In **d** with Angelo-EAM [110], Foiles-EAM [111], and Zhou-EAM [112] potentials, the redissociated dislocation is absorbed by the CTB, with two partials gliding on the twin plane in opposite directions. Adapted with permission from Ref. [84]

acts as a barrier to dislocation motion; (ii) in Al, the leading segment is absorbed and glides on the CTB, which acts as sinks for lattice dislocations. In particular for Al, four dislocation/CTB interaction modes are identified, which are affected by applied shear stress, dislocation line length, and dislocation line curvature. This study highlights the complexity of dislocation/GB interactions, as well as the significance to let dislocations evolve freely in 3D and to probe the mechanisms of slip transfer in polycrystalline and twinned metals using sufficiently large models. In comparison, prior atomistic simulations in the literature [106] are limited to a small set of simulation parameters: low applied shear stresses and short/straight dislocation lines enforced by PBCs.

In Ni, five EAM potentials [108–112] were employed in CAC simulations of dislocation/GB interactions [84]. For the  $\Sigma 3$  CTB, the leading screw segment is transmitted into the twinned grain using two interatomic potentials (Fig. 12.6d), but is absorbed and glides on the CTB when the other three potentials are employed (Fig. 12.6e). In both reactions, each dislocation always follows the recombination-redissociation process, without forming any CTB dislocations in the process of recombination, as shown in Fig. 12.6c. For the  $\Sigma 11$  STGB, however,

all five EAM potential fits predict dislocation absorption, during which the leading partial dislocation in the incoming grain splits into a STGB partial dislocation and a stair-rod type dislocation, which subsequently reacts with the trailing partial dislocation in the incoming grain to form another STGB partial dislocation. This work highlights the uncertainty in computed dislocation-interface reactions associated with the deployment of a variety of interatomic potentials and suggests that the applicability of dislocation/GB interaction criteria in the literature derived from limited studies may be limited [106].

## 12.5 Conclusions

In this chapter, we first review the basics of GCM in Sect. 12.1 and establish, in accordance with the insights of Maugin, that GCM is a better approximation than CCM to the description of real materials. In Sect. 12.2, the theoretical foundations and governing equations of AFT are introduced, in comparison with several representative CG models in the literature. Fundamentally different from CG particle models and most field theories such as the micromorphic theory, AFT views a material as a continuous collection of material points, while embedded within each point there is a group of discrete atoms, providing an analytical link between the continuum quantities and the atomic variable. In Sect. 12.3, we discuss important aspects of the AFT-based CAC approach, including its advantages relative to other multiscale modeling methods, code development, and numerical implementations. Applications of CAC to metal plasticity are reviewed in Sect. 12.4, with an emphasis on static dislocation properties, fast moving dislocations and phonons, as well as dislocation/GB interactions. It is shown that CAC provides largely satisfactory predictive results at a fraction of the computational cost of the fully atomistic version of the same models.

The CAC applications discussed in this chapter, as well as all others in the last decade, establish that the CAC method is useful at intermediate length scales between fully-resolved atomistics and mesoscale modeling approaches such as DD, phase field method, and CPFEM. In this regard, CAC can serve as a complement to methods at the lower and higher length scales. The CAC method is especially useful to explore problems in which full atomistic resolution is required in some regions (e.g., complex atomistic phenomena involving dislocations reactions with other defects), with coarse-graining employed elsewhere to support representation of dislocation interactions and transport. In such cases, dislocation lines span between fully resolved atomistic and coarse-grained domains with the same constitutive equation used everywhere. Compared with MD/MS, CAC is advantageous in that with greatly reduced DOFs, the key characteristics of complex dislocation behavior can be reasonably well described, despite the coarse-graining errors. Compared with DD, in which only the dislocation lines are resolved, CAC simulations contain more DOFs and are less computationally efficient; however, CAC resolves dislocation core effects explicitly, in addition to long-range elastic interactions.

It is anticipated that CAC may assist in computational techniques at higher length scales by providing useful guidance regarding the form of higher scale constitutive models.

Future applications of the CAC method to metal plasticity include slip transfer of more general dislocation types with different curvatures across more general GBs, the “valve effect” in fracture [113], and dislocation substructure evolution [114]. In terms of the methodological development, we will implement higher order shape/interpolation functions and/or enrichment functions within elements to admit dislocations in element interior regions, as well as design adaptive mesh refinement schemes for dislocation migration. For finite temperature dynamic problems, the next step is to develop a novel description of the temperature in the coarse-grained domain such that it is consistent with that in MD [25]. Another future extension, which is more challenging, is to advance non-equilibrium finite temperature dynamic CAC for non-conservative systems, requiring the implementation of the balance equation of energy (Eq. 12.4).

**Acknowledgements** These results are in part based upon work supported by the National Science Foundation as a collaborative effort between Georgia Tech (CMMI-1232878) and University of Florida (CMMI-1233113). Any opinions, findings, and conclusions or recommendations expressed in this material are those of the authors and do not necessarily reflect the views of the National Science Foundation. The authors thank Dr. Jinghong Fan, Dr. Qian Deng, Dr. Shengfeng Yang, Dr. Xiang Chen, Mr. Rui Che, and Mr. Weixuan Li for helpful discussions, Mr. Kevin Chu for building the Python scripting interface in PyCAC, and Dr. Aleksandr Blekh for arranging execution of PyCAC via MATIN. The work of SX was supported in part by Georgia Tech Institute for Materials and in part by the Elings Prize Fellowship in Science offered by the California NanoSystems Institute (CNSI) on the UC Santa Barbara campus. SX also acknowledges support from the Center for Scientific Computing from the CNSI, MRL: an NSF MRSEC (DMR-1121053). LX acknowledges the support from the Department of Energy, Office of Basic Energy Sciences under Award Number DE-SC0006539. The work of LX was also supported in part by the National Science Foundation under Award Number CMMI-1536925. DLM is grateful for the additional support of the Carter N. Paden, Jr. Distinguished Chair in Metals Processing. This work used the Extreme Science and Engineering Discovery Environment (XSEDE), which is supported by National Science Foundation grant number ACI-1053575.

## References

1. Maugin, G.A.: *Non-Classical Continuum Mechanics: A Dictionary*. Springer, Singapore (2016)
2. Maugin, G.A.: Some remarks on generalized continuum mechanics. *Math. Mech. Solids* **20**(3), 280–291 (2015)
3. Maugin, G.A.: Generalized continuum mechanics: various paths. In: *Continuum Mechanics Through the Twentieth Century*, pp. 223–241. Springer (2013)
4. Maugin, G.A.: *Continuum Mechanics Through the Twentieth Century*, *Solid Mechanics and Its Applications*, vol. 196, pp. 978–994. Springer, Berlin (2013)
5. Maugin, G.A.: Generalized continuum mechanics: what do we mean by that? In: Maugin, G., Metrikine, A. (eds.) *Mechanics of Generalized Continua. Advances in Mechanics and Mathematics*, pp. 3–13. Springer, New York, NY (2010)

6. Maugin, G.A.: A historical perspective of generalized continuum mechanics. In: Altenbach, H., Maugin, G., Erofeev, V. (eds.) *Mechanics of Generalized Continua*. Advanced Structured Materials, vol. 7. pp. 3–19 (2011)
7. Maugin, G.A., Metrikine, A.V.: *Mechanics of Generalized Continua: One Hundred Years After the Cosserats*. Springer, New York (2010)
8. Chen, Y., Lee, J.: Atomistic formulation of a multiscale field theory for nano/micro solids. *Philos. Mag.* **85**(33–35), 4095–4126 (2005)
9. Chen, Y.: Reformulation of microscopic balance equations for multiscale materials modeling. *J. Chem. Phys.* **130**(13), 134706 (2009)
10. Chen, Y., Lee, J., Xiong, L.: A generalized continuum theory and its relation to micromorphic theory. *J. Eng. Mech.* **135**(3), 149–155 (2009)
11. Chen, Y., Zimmerman, J., Krivtsov, A., McDowell, D.L.: Assessment of atomistic coarse-graining methods. *Int. J. Eng. Sci.* **49**(12), 1337–1349 (2011)
12. Cosserat, E., Cosserat, F.: *Théorie des corps déformables*, vol. 3, pp. 17–29, Paris (1909)
13. Chen, Y., Lee, J.D., Eskandarian, A.: Micropolar theory and its applications to mesoscopic and microscopic problems. *Comput. Model. Eng. Sci.* **5**(1), 35–43 (2004)
14. Eringen, A.C.: Theory of micropolar elasticity. In: *Microcontinuum Field Theories*, pp. 101–248. Springer (1999)
15. Eringen, A.C.: *Microcontinuum Field Theories: I. Foundations and Solids*. Springer, New York (1999)
16. Eringen, A.C.: *Mechanics of Micromorphic Continua*. Springer (1968)
17. Chen, Y., Lee, J.D.: Connecting molecular dynamics to micromorphic theory. (I). Instantaneous and averaged mechanical variables. *Phys. A* **322**, 359–376 (2003)
18. Chen, Y., Lee, J.D.: Connecting molecular dynamics to micromorphic theory. (II). Balance laws. *Phys. A* **322**, 377–392 (2003)
19. Chen, Y., Lee, J., Eskandarian, A.: Atomistic counterpart of micromorphic theory. *Acta Mech.* **161**(1–2), 81–102 (2003)
20. Chen, Y., Lee, J.D.: Determining material constants in micromorphic theory through phonon dispersion relations. *Int. J. Eng. Sci.* **41**(8), 871–886 (2003)
21. Chen, Y., Lee, J.D., Eskandarian, A.: Atomistic viewpoint of the applicability of microcontinuum theories. *Int. J. Solids Struct.* **41**(8), 2085–2097 (2004)
22. Chen, Y., Lee, J.D., Eskandarian, A.: Examining the physical foundation of continuum theories from the viewpoint of phonon dispersion relation. *Int. J. Eng. Sci.* **41**, 61–83 (2003)
23. Hoover, W.G.: *Computational Statistical Mechanics*. Elsevier (1991)
24. Chen, Y.: Local stress and heat flux in atomistic systems involving three-body forces. *J. Chem. Phys.* **124**(5), 054113 (2006)
25. Chen, Y., Diaz, A.: Local momentum and heat fluxes in transient transport processes and inhomogeneous systems. *Phys. Rev. E* **94**(5), 053309 (2016)
26. Chen, Y.: The origin of the distinction between microscopic formulas for stress and Cauchy stress. *EPL* **116**(3), 34003 (2016)
27. Espanol, P.: Statistical mechanics of coarse-graining. In: *Novel Methods in Soft Matter Simulations*, pp. 69–115. Springer (2004)
28. Izvekov, S., Voth, G.A.: Multiscale coarse-graining of liquid-state systems. *J. Chem. Phys.* **123**(13), 134105 (2005)
29. Izvekov, S., Voth, G.A.: A multiscale coarse-graining method for biomolecular systems. *J. Phys. Chem. B* **109**(7), 2469–2473 (2005)
30. Noid, W., Chu, J.W., Ayton, G.S., Krishna, V., Izvekov, S., Voth, G.A., Das, A., Andersen, H.C.: The multiscale coarse-graining method. I. A rigorous bridge between atomistic and coarse-grained models. *J. Chem. Phys.* **128**(24), 244114 (2008)
31. Noid, W., Liu, P., Wang, Y., Chu, J.W., Ayton, G.S., Izvekov, S., Andersen, H.C., Voth, G.A.: The multiscale coarse-graining method. II. Numerical implementation for coarse-grained molecular models. *J. Chem. Phys.* **128**(24), 244115 (2008)
32. Tadmor, E.B., Ortiz, M., Phillips, R.: Quasicontinuum analysis of defects in solids. *Philos. Mag. A* **73**, 1529–1563 (1996)

33. Dupuy, L.M., Tadmor, E.B., Miller, R.E., Phillips, R.: Finite-temperature quasicontinuum: molecular dynamics without all the atoms. *Phys. Rev. Lett.* **95**, 060202 (2005)
34. Kulkarni, Y., Knap, J., Ortiz, M.: A variational approach to coarse-graining of equilibrium and non-equilibrium atomistic description at finite temperature. *J. Mech. Phys. Solids* **56**, 1417–1449 (2008)
35. Shenoy, V.B., Miller, R., Tadmor, E.B., Phillips, R., Ortiz, M.: Quasicontinuum models of interfacial structure and deformation. *Phys. Rev. Lett.* **80**, 742–745 (1998)
36. Rudd, R.E., Broughton, J.Q.: Coarse-grained molecular dynamics and the atomic limit of finite elements. *Phys. Rev. B* **58**(10), R5893 (1998)
37. Irving, J., Kirkwood, J.G.: The statistical mechanical theory of transport processes. IV. The equations of hydrodynamics. *J. Chem. Phys.* **18**(6), 817–829 (1950)
38. Kittel, C.: *Introduction to Solid State Physics*. Wiley, Inc (1956)
39. Deng, Q., Xiong, L., Chen, Y.: Coarse-graining atomistic dynamics of fracture by finite element method. *Int. J. Plast.* **26**(9), 1402–1414
40. Xiong, L., Chen, Y.: Coarse-grained simulations of single-crystal silicon. *Modell. Simul. Mater. Sci. Eng.* **17**, 035002 (2009)
41. Xiong, L., Chen, Y., Lee, J.D.: Atomistic simulation of mechanical properties of diamond and silicon carbide by a field theory. *Model. Simul. Mater. Sci. Eng.* **15**(5), 535 (2007)
42. Xiong, L., Tucker, G., McDowell, D.L., Chen, Y.: Coarse-grained atomistic simulation of dislocations. *J. Mech. Phys. Solids* **59**(2), 160–177 (2011)
43. Xu, S., Che, R., Xiong, L., Chen, Y., McDowell, D.L.: A quasistatic implementation of the concurrent atomistic-continuum method for FCC crystals. *Int. J. Plast.* **72**, 91–126 (2015)
44. Xu, S., Payne, T.G., Chen, H., Liu, Y., Xiong, L., Chen, Y., McDowell, D.L.: PyCAC: The concurrent atomistic-continuum simulation environment. *J. Mater. Res.* (2018) in press, <https://doi.org/10.1557/jmr.2018.8>
45. Shilkrot, L.E., Curtin, W.A., Miller, R.E.: A coupled atomistic/continuum model of defects in solids. *J. Mech. Phys. Solids* **50**, 2085–2106 (2002)
46. Shilkrot, L.E., Miller, R.E., Curtin, W.A.: Coupled atomistic and discrete dislocation plasticity. *Phys. Rev. Lett.* **89**, 025501 (2002)
47. Xu, S., Xiong, L., Deng, Q., McDowell, D.L.: Mesh refinement schemes for the concurrent atomistic-continuum method. *Int. J. Solids Struct.* **90**, 144–152 (2016)
48. Zbib, H.M., de la Rubia, T.D., Bulatov, V.: A multiscale model of plasticity based on discrete dislocation dynamics. *ASME J. Eng. Mater. Technol.* **124**(1), 78–87 (2002)
49. Hochrainer, T., Zaiser, M., Gumbsch, P.: A three-dimensional continuum theory of dislocation systems: kinematics and mean-field formulation. *Philos. Mag.* **87**, 1261–1282 (2007)
50. Arsenlis, A., Cai, W., Tang, M., Rhee, M., Opperstrup, T., Hommes, G., Pierce, T.G., Bulatov, V.V.: Enabling strain hardening simulations with dislocation dynamics. *Model. Simul. Mater. Sci. Eng.* **15**, 553–595 (2007)
51. El-Azab, A., Deng, J., Tang, M.: Statistical characterization of dislocation ensembles. *Philos. Mag.* **87**(8–9), 1201–1223 (2007)
52. Devincere, B., Hoc, T., Kubin, L.: Dislocation mean free paths and strain hardening of crystals. *Science* **320**(5884), 1745–1748 (2008)
53. Motz, C., Weygan, D., Senger, J., Gumbsch, P.: Initial dislocation structures in 3-D discrete dislocation dynamics and their influence on microscale plasticity. *Acta Mater.* **57**(6), 1744–1754 (2009)
54. Zaiser, M., Sandfeld, S.: Scaling properties of dislocation simulations in the similitude regime. *Model. Simul. Mater. Sci. Eng.* **22**:065012, (2014)
55. Groma, I., Zaiser, M., Ispanovity, P.D.: Dislocation patterning in a two-dimensional continuum theory of dislocations. *Phys. Rev. B* **93**, 214110 (2016)
56. Xia, S., El-Azab, A.: Computational modelling of mesoscale dislocation patterning and plastic deformation of single crystals. *Model. Simul. Mater. Sci. Eng.* **23**(5), 55009 (2015)
57. Xiong, L., Chen, Y.: Effects of dopants on the mechanical properties of nanocrystalline silicon carbide thin film. *Comput. Model. Eng. Sci.* **24**, 203–214 (2008)

58. Xiong, L., Chen, Y.: Coarse-grained simulations of single-crystal silicon. *Model. Simul. Mater. Sci. Eng.* **17**, 035002 (2009)
59. Deng, Q., Chen, Y.: A coarse-grained atomistic method for 3D dynamic fracture simulation. *Int. J. Multiscale Comput. Eng.* **11**, 227–237 (2013)
60. Xiong, L., Deng, Q., Tucker, G., McDowell, D.L., Chen, Y.: A concurrent scheme for passing dislocations from atomistic to continuum domains. *Acta Mater.* **60**, 899–913 (2012)
61. Xiong, L., Deng, Q., Tucker, G., McDowell, D.L., Chen, Y.: Coarse-grained atomistic simulations of dislocations in Al, Ni and Cu crystals. *Int. J. Plast.* **38**, 86–101 (2012)
62. Xiong, L., McDowell, D.L., Chen, Y.: Nucleation and growth of dislocation loops in Cu, Al and Si by a concurrent atomistic-continuum method. *Scr. Mater.* **67**, 633–636 (2012)
63. Xiong, L., Chen, Y.: Coarse-grained atomistic modeling and simulation of inelastic material behavior. *Acta Mech. Solida Sin.* **25**, 244–261 (2012)
64. Xiong, L., McDowell, D.L., Chen, Y.: Sub-THz Phonon drag on dislocations by coarse-grained atomistic simulations. *Int. J. Plast.* **55**, 268–278 (2014)
65. Xiong, L., Xu, S., McDowell, D.L., Chen, Y.: Concurrent atomistic-continuum simulations of dislocation-void interactions in fcc crystals. *Int. J. Plast.* **65**, 33–42 (2015)
66. Xiong, L., Rigelesaiyin, J., Chen, X., Xu, S., McDowell, D.L., Chen, Y.: Coarse-grained elastodynamics of fast moving dislocations. *Acta Mater.* **104**, 143–155 (2016)
67. Yang, S., Xiong, L., Deng, Q., Chen, Y.: Concurrent atomistic and continuum simulation of strontium titanate. *Acta Mater.* **61**, 89–102 (2013)
68. Yang, S., Chen, Y.: Concurrent atomistic and continuum simulation of bi-crystal strontium titanate with tilt grain boundary. *Proc. Roy. Soc. A* **471**, 20140758 (2015)
69. Yang, S., Zhang, N., Chen, Y.: Concurrent atomistic-continuum simulation of polycrystalline strontium titanate. *Philos. Mag.* **95**, 2697–2716 (2015)
70. Yang, S., Chen, Y.: Concurrent atomistic-continuum simulation of defects in polyatomic ionic materials. In: Weinberger, C., Tucker, G. (eds.) *Multiscale Materials Modeling for Nanomechanics*. Springer International Publishing, Switzerland (2016)
71. Chen, X., Xiong, L., McDowell, D.L., Chen, Y.: Effects of phonons on mobility of dislocations and dislocation arrays. *Scr. Mater.* **137**, 22–26 (2017)
72. Chen, X., Li, W., Xiong, L., Li, Y., Yang, S., Zheng, Z., McDowell, D.L., Chen, Y.: Ballistic-diffusive phonon heat transport across grain boundaries. *Acta Mater.* **136**, 355–365 (2017)
73. Chen, X., Diaz, A., Xiong, L., Chen, Y.: Passing waves from atomistic to continuum. *J. Comput. Phys.* **354**, 393–402 (2018)
74. Chen, X., Li, W., Diaz, A., Li, Y., McDowell, D.L., Chen, Y.: Recent progress in the concurrent atomistic-continuum method and its application in phonon transport. *MRS Commun.* **7**(4), 785–797 (2017)
75. Li, J.: AtomEye: an efficient atomistic configuration viewer. *Model. Simul. Mater. Sci. Eng.* **11**(2), 173 (2003)
76. Stukowski, A.: Visualization and analysis of atomistic simulation data with OVITO—the Open Visualization Tool. *Model. Simul. Mater. Sci. Eng.* **18**(1), 015012 (2010)
77. Jones, J.E.: On the determination of molecular fields. II. From the equation of state of a gas. *Proc. R. Soc. Lond. A* **106**(738), 463–477 (1924)
78. Daw, M.S., Baskes, M.I.: Embedded-atom method: derivation and application to impurities, surfaces, and other defects in metals. *Phys. Rev. B* **29**(12), 6443–6453 (1984)
79. Xu, S.: The concurrent atomistic-continuum method: Advancements and applications in plasticity of face-centered cubic metals. Ph.D. Dissertation, Georgia Institute of Technology (2016)
80. Allen, M.P., Tildesley, D.J.: *Computer Simulation of Liquids*. Oxford University Press, USA (1989)
81. Verlet, L.: Computer “experiments” on classical fluids. I. Thermodynamical properties of Lennard-Jones molecules. *Phys. Rev.* **159**, 98–103 (1967)

82. Swope, W.C., Andersen, H.C., Berens, P.H., Wilson, K.R.: A computer simulation method for the calculation of equilibrium constants for the formation of physical clusters of molecules: Application to small water clusters. *J. Chem. Phys.* **76**(1), 637–649 (1982)
83. Xu, S., Xiong, L., Chen, Y., McDowell, D.L.: Sequential slip transfer of mixed-character dislocations across  $\Sigma 3$  coherent twin boundary in FCC metals: A concurrent atomistic-continuum study. *npj Comput. Mater.* **2**, 15016 (2016)
84. Xu, S., Xiong, L., Chen, Y., McDowell, D.L.: A concurrent atomistic-continuum study of slip transfer of sequential mixed character dislocations across symmetric tilt grain boundaries in Ni. *JOM* **69**, 814–821 (2017)
85. McDowell, D.L.: A perspective on trends in multiscale plasticity. *Int. J. Plast.* **26**, 1280–1309 (2010)
86. Xu, S., Xiong, L., Chen, Y., McDowell, D.L.: An analysis of key characteristics of the Frank-Read source process in FCC metals. *J. Mech. Phys. Solids* **96**, 460–476 (2016)
87. Xu, S., Xiong, L., Chen, Y., McDowell, D.L.: Shear stress- and line length-dependent screw dislocation cross-slip in FCC Ni. *Acta Mater.* **122**, 412–419 (2017)
88. Xu, S., Xiong, L., Chen, Y., McDowell, D.L.: Edge dislocations bowing out from a row of collinear obstacles in Al. *Scr. Mater.* **123**, 135–139 (2016)
89. Xu, S., Xiong, L., Chen, Y., McDowell, D.L.: Validation of the concurrent atomistic-continuum method on screw dislocation/stacking fault interactions. *Crystals* **7**, 120 (2017)
90. Xiong, L., Chen, X., Zhang, N., McDowell, D.L., Chen, Y.: Prediction of phonon properties of 1D polyatomic systems using concurrent atomistic-continuum simulation. *Arch. Appl. Mech.* **84**, 1665–1675 (2014)
91. Rice, J.R.: Inelastic constitutive relations for solids: An internal variable theory and its application to metal plasticity. *J. Mech. Phys. Solids* **19**, 433–455 (1971)
92. Muschik, W.: *Non-Equilibrium Thermodynamics with Application to Solids*. Springer, New York (1993)
93. Hull, D., Bacon, D.J.: *Introduction to Dislocations*, 5th edn. Butterworth-Heinemann, Oxford, UK (2011)
94. Anderson, P.M., Hirth, J.P., Lothe, J.: *Theory of Dislocations*, 3rd edn. Cambridge University Press (2017)
95. Nye, J.F.: Some geometrical relations in dislocated crystals. *Acta Mater.* **1**(2), 153–162 (1953)
96. Hill, R., Sneddon, I.N. (eds.): *Progress in Solid Mechanics*, vol. 1, p. 330. North-Holland Publishing Company (1960)
97. Mishin, Y., Mehl, M.J., Papaconstantopoulos, D.A., Voter, A.F., Kress, J.D.: Structural stability and lattice defects in copper: Ab initio, tight-binding, and embedded-atom calculations. *Phys. Rev. B* **63**(22), 224106 (2001)
98. Plimpton, S.: Fast parallel algorithms for short-range molecular dynamics. *J. Comput. Phys.* **117**, 1–19 (1995)
99. Hirel, P.: AtomsK: A tool for manipulating and converting atomic data files. *Comput. Phys. Commun.* **197**, 212–219 (2015)
100. Hartley, C.S., Mishin, Y.: Representation of dislocation cores using Nye tensor distributions. *Mater. Sci. Eng. A* **400**, 18–21 (2005)
101. Gurrutxaga-Lerma, B., Balint, D.S., Dini, D., Eakins, D.E., Sutton, A.P.: A dynamic discrete dislocation plasticity method for the simulation of plastic relaxation under shock loading. *Proc. R. Soc. A* **469**, 20130141 (2013)
102. Chen, X., Chernatynskiy, A., Xiong, L., Chen, Y.: A coherent phonon pulse model for transient phonon thermal transport. *Comput. Phys. Commun.* **195**, 112–116 (2015)
103. Ramesh, K.T.: *Nanomaterials: Mechanics and Mechanisms*. Springer (2009)
104. Kacher, J., Eftink, B.P., Cui, B., Robertson, I.M.: Dislocation interactions with grain boundaries. *Curr. Opin. Solid State Mater. Sci.* **18**, 227–243 (2014)
105. Counts, W.A., Braginsky, M.V., Battaile, C.C., Holm, E.A.: Predicting the Hall-Petch effect in fcc metals using non-local crystal plasticity. *Int. J. Plast.* **24**, 1243–1263 (2008)

106. Spearot, D.E., Sangid, M.D.: Insights on slip transmission at grain boundaries from atomistic simulations. *Curr. Opin. Solid State Mater. Sci.* **18**, 188–195 (2014)
107. Stukowski, A.: Structure identification methods for atomistic simulations of crystalline materials. *Model. Simul. Mater. Sci. Eng.* **20**, 045021 (2012)
108. Mishin, Y., Farkas, D., Mehl, M.J., Papaconstantopoulos, D.A.: Interatomic potentials for monoatomic metals from experimental data and ab initio calculations. *Phys. Rev. B* **59**, 3393 (1999)
109. Voter, A.F., Chen, S.P.: Accurate interatomic potentials for Ni, Al, and Ni<sub>3</sub>Al. *Mater. Res. Soc. Symp. Proc.* **82**, 175 (1987)
110. Angelo, J.E., Moody, N.R., Baskes, M.I.: Trapping of hydrogen to lattice-defects in nickel. *Model. Simul. Mater. Sci. Eng.* **3**, 289 (1995)
111. Foiles, S.M., Hoyt, J.J.: Computation of grain boundary stiffness and mobility from boundary fluctuations. *Acta Mater.* **54**, 3351 (2006)
112. Zhou, X.W., Johnson, R.A., Wadley, H.N.G.: Misfit-energy-increasing dislocations in vapor-deposited CoFe/NiFe multilayers. *Phys. Rev. B* **69**, 144113 (2004)
113. Lipkin, D.M., Clarke, D.R., Beltz, G.E.: A strain-gradient model of cleavage fracture in plastically deforming materials. *Acta Mater.* **44**, 4051–4058 (1996)
114. Hussein, A.M., El-Awady, J.A.: Quantifying dislocation microstructure evolution and cyclic hardening in fatigued face-centered cubic single crystals. *J. Mech. Phys. Solids* **91**, 126–144 (2016)